Dual High-Energy X-ray Digital Radiography for Material Discrimination in Cargo Containers

Sanjeevareddy KOLKOORI, Norma WROBEL,
Andreas DERESCH, Bernhard REDMER, Uwe EWERT

BAM Federal Institute for Materials Research and Testing; Berlin, Germany
Phone: +49 30 8104 4104, Fax: +49 30 8104 4657; e-mail: sanjeevareddy.kolkoori@bam.de

Abstract
In this contribution, we present a dual high-energy X-ray imaging technique for cargo container inspection using the "spectral high-energy X-ray attenuation method". This method is based on attenuation of continuous high-energy spectra. The developed experimental technique consists of a betatron as high-energy (up to 7.5 MeV) X-ray source and a matrix detector with high spatial resolution (400 µm) for digital X-ray imaging. In order to evaluate the material discrimination capability using dual high-energy X-ray imaging, a test specimen is proposed, comprising step wedges of different low and high atomic number (Z) materials. The selected X-ray spectra for the dual-energy experiments correspond to 3 MV and 7.5 MV acceleration potential of the betatron. We evaluated the ratio between low- and high-energy X-ray attenuation coefficients quantitatively based on simulated poly-energetic high-energy X-ray source spectra and the detector sensitivity using the "analytical Radiographic Testing inspection simulation tool" (aRTist) developed at BAM. The simulated effective attenuation coefficients are compared with corresponding experimental results in order to establish a method for identification of low- and high-Z materials in the container. Finally, important applications of the proposed technique in the context of aviation security are discussed.

Keywords: digital radiography, NDT, high-energy X-ray imaging, betatron, digital detector array (DDA), container inspection, material discrimination, effective attenuation coefficient

1. Introduction

Radiological methods are non-destructive testing and evaluation (NDT&E) methods to detect dangerous and contraband materials in large objects. Dual low-energy (<450 keV) X-ray imaging is a well-established technique in the medical field and for baggage scanning applications at airports [1,2,3,4]. Generally, medical dual-energy systems and baggage scanners operate with acceleration potentials between 80 kV and 160 kV. The corresponding X-ray spectra are well separated, resulting in the dominance of either photoelectric absorption or the Compton effect for many materials. In addition, for typical applications the effective mass attenuation coefficient is strongly dependent on the atomic number (Z). This leads to lower complexity in material discrimination. Whereas in the case of large, densely packed air-cargo container inspection, the radiation beam penetrates several meters, resulting in a strong dependence of the effective attenuation coefficient μ_{eff} on the material thickness. Furthermore, due to the decreased separation between high-energy (>1 MeV) X-ray spectra, μ_{eff} is less dependent on Z, but shows strong dependence on the material density variations.

When compared to conventional (<450 keV) X-ray imaging, high-energy (>1 MeV) digital radiography (DR) is required for the NDT of densely packed steel containers because of the high penetration capability through thick objects and the ability to distinguish between low- and high-Z materials based on the balance between the Compton effect and pair production. For this purpose, industrial NDT high-energy X-ray sources are available, such as linear accelerators (linac) [5,6] and portable X-ray betatrons [7,8], which are suitable for inspection of large objects. The reason for selecting an X-ray betatron as the high-energy X-ray source for our present investigations is due to its ability to penetrate 350 mm of steel or 1.5 m of heterogeneous concrete structures. Additionally, due to the comparatively small size of its focal spot (1.5×3 mm^2 derived from measurements), the digital image quality can be

improved significantly. Furthermore, no special cooling systems are necessary, making it highly suitable for mobile NDT applications. Recent investigations with Digital Detector Arrays (DDAs) have shown the improvement of essential image quality parameters such as image basic spatial resolution (SR_b) and signal-to-noise ratio (SNR) [9,10]. These main advantages of high resolution DDAs are considered in the presented experimental technique.

The aim of this paper is threefold. First, we discuss dual high-energy X-ray imaging using the continuous-spectrum high-energy X-ray attenuation method. Then, we present numerical results for the dual-energy function, which describes the ratio between low- and high-energy X-ray attenuation coefficients. Next, we compare experimental and simulated dual-energy images of a test phantom containing different low- and high-Z step wedges. Finally, important applications of the proposed technique to the aviation security are discussed.

2. Theory: Dual High-Energy X-ray Imaging

The energy-dependent incident and transmitted X-ray intensities for an object illuminated by a poly-energetic X-ray beam are expressed in terms of the continuous X-ray source spectrum *S(E)* and the detector sensitivity *D(E)*,

$$\text{Incident intensity: } I_0 = \int_{E=0}^{E_{max}} S(E)\cdot D(E)\,dE \quad \text{..... (1)}$$

$$\text{Transmitted Intensity: } I = \int_{E=0}^{E_{max}} S(E)\cdot D(E)\,e^{-\mu(E)\cdot t}\,dE \quad \text{..... (2)}$$

The total spectral attenuation coefficient is derived using the Beer-Lambert law and is given as [11,12]

$$\mu = \frac{-1}{t}\left(\log\left(\frac{I}{I_0}\right)\right) = \frac{-1}{t}\left(\log\left(\frac{\int_{E=0}^{E_{max}} S(E)\cdot D(E)\,e^{-\mu(E)\cdot t}\,dE}{\int_{E=0}^{E_{max}} S(E)\cdot D(E)\,dE}\right)\right) \quad \text{..... (3)}$$

$$= \frac{-1}{t}\left(\log\left(\int_{E=0}^{E_{max}} W(E)\,e^{-\mu(E)\cdot t}\,dE\right)\right)$$

with the weighting function

$$W(E) = \frac{S(E)\cdot D(E)}{\int_{E=0}^{E_{max}} S(E)\cdot D(E)\,dE} \quad \text{..... (4)}$$

The poly-energetic X-ray spectra for low energy (3 MV) and high energy (7.5 MV), simulated using the "analytical Radiographic Testing inspection simulation tool" (aRTist) [13,14,15], are shown in figure 1. The detector sensitivity *D(E)* is defined as the product of photon interaction probability and average photon energy transfer per interaction for an incident photon of energy *E*. The energy-dependence of the detector sensitivity *D(E)* has been calculated for the Gd_2O_2S scintillator used in the experiments and is shown in figure 2. The main aim of this analytical study was to understand the dependence of the effective attenuation coefficient μ_{eff} on the material's atomic number (Z) at higher X-ray energies.

2.1 Thickness-independent dual-energy function

For shorter paths (i.e. penetration through smaller objects) of the X-rays, the total linear attenuation-coefficient is given by [11],

$$\mu = \int_{E=0}^{E_{\max}} W(E)\,\mu(\mathrm{E})\,dE \quad \text{..... (5)}$$

For dual-energy measurements at conventional energies, the ratio of the effective linear attenuation coefficients for the low-energy spectrum μ_{Low} and for the high-energy spectrum μ_{High} can be obtained by

$$\mathrm{F(Z)} = \frac{\mu_{Low}(Z)}{\mu_{High}(Z)} = \left(\frac{\int_{E_1=0}^{E_{\max}} W(E_1)\,\mu(\mathrm{E}_1, Z)\,dE_1}{\int_{E_2=0}^{E_{\max}} W(E_2)\,\mu(\mathrm{E}_2, Z)\,dE_2} \right) \quad \text{..... (6)}$$

The above method is independent of the thickness of the object being inspected.

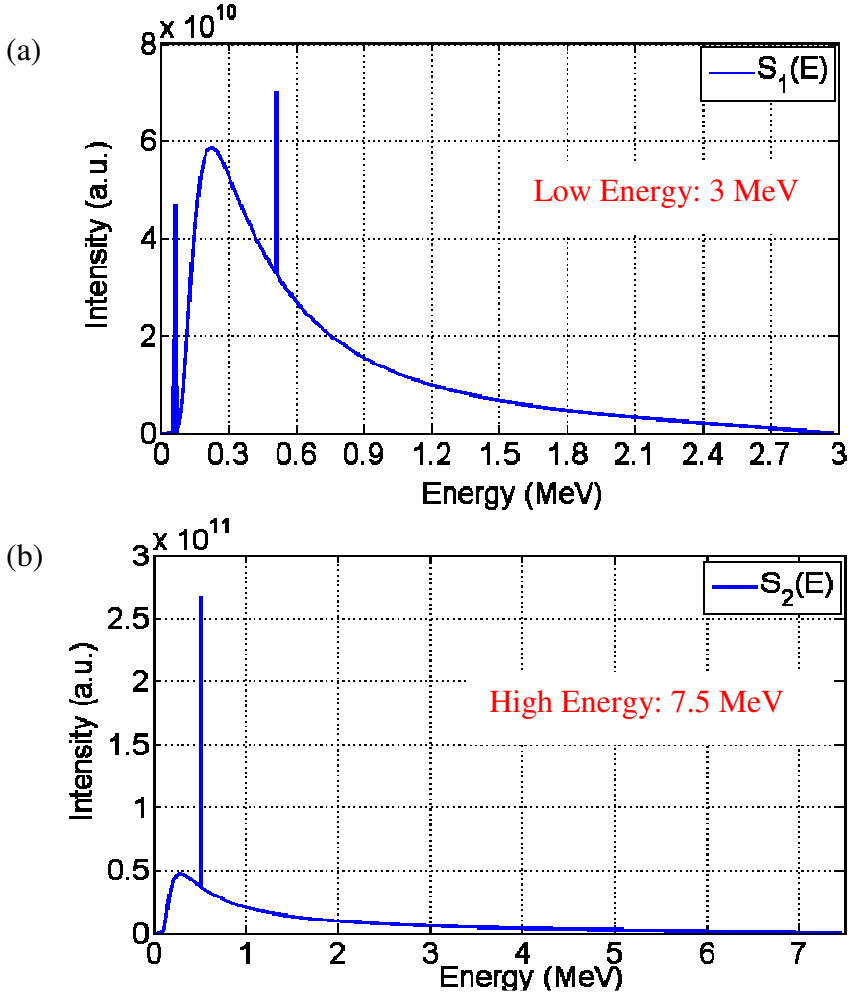

Figure 1. Poly-energetic betatron X-ray spectra for source potential (a) 3 MeV with 4 mm thick Cu pre-filter and (b) 7.5 MeV with 10 mm thick Cu pre-filter, both simulated using aRTist.

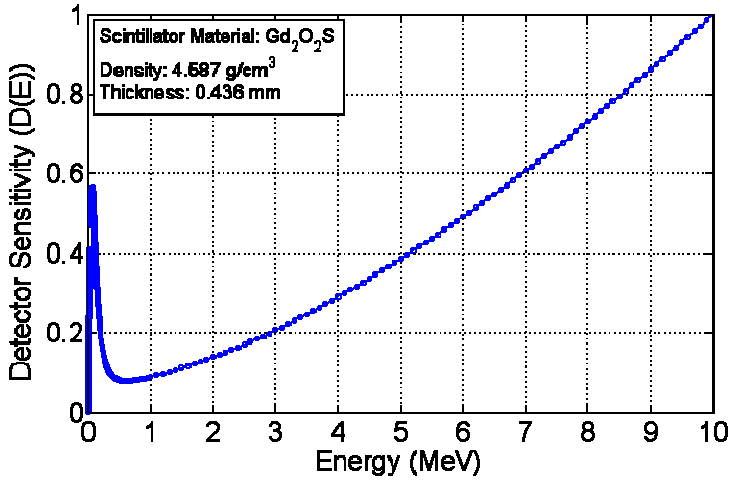

Figure 2. The calculated detector efficiency *D(E)* for the Gd_2O_2S scintillator used in the dual high-energy measurements.

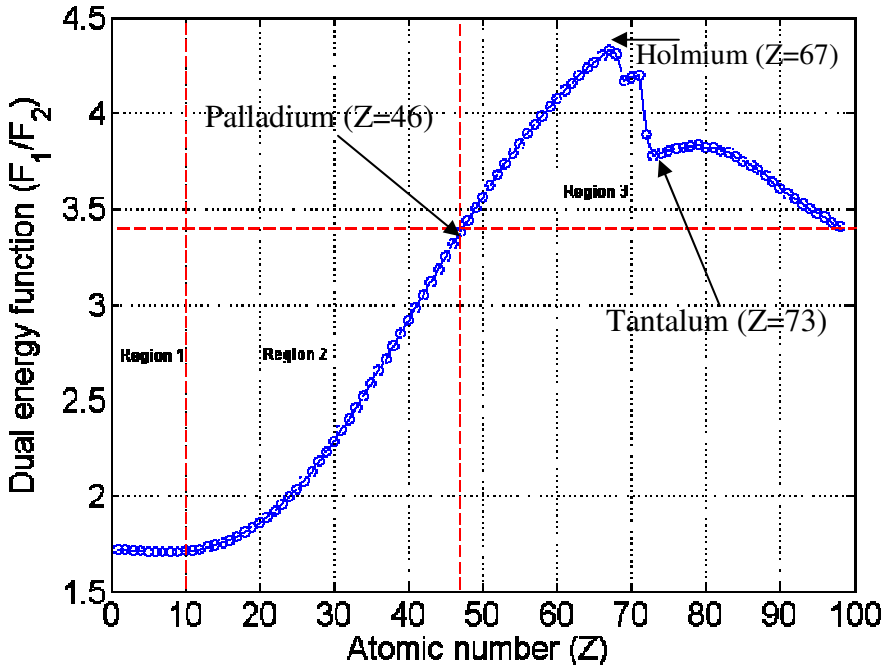

Figure 3. Variation of dual-energy function F(Z) with atomic number. The selected low- and high-energy spectra correspond to 3 MV and 7.5 MV, respectively.

Figure 3 shows the dependence of the dual-energy function on material atomic number (Z). The following important points can be noticed in the obtained plot:

The behavior of the dual-energy function F(Z), as shown in fig. 3, is divided into three regions. Region 1 corresponds to low Z materials (Z<=10) where most of the dangerous materials appear. F(Z) in this region is nearly constant. Hence, material discrimination is not possible between low Z materials. Whereas, F(Z) varies monotonically with Z in region 2 (i.e. Z>10 and Z<=46). As a result, there is a possibility of material discrimination within region 2, as well as compared to the other regions. Region 3 corresponds to atomic-numbers Z>46 where F(Z) shows similar values for materials with different Z. Consequently, difficulties occur in discriminating heavy metals using dual high-energy X-ray imaging. Furthermore, two sharp dips can be seen near tantalum (Z=73), because the low-energy spectrum includes features characteristic for this material, as it is used for the target in the betatron X-ray source.

2.2 Thickness-dependent dual-energy function

Generally, in the case of inspection of large cargo containers, the X-ray beam penetrates through dense objects and takes longer ray paths (on the order of meters). Consequently, the dual-energy function F(Z) not only depends on the material's atomic number (Z), but also on the material thickness.

For dual high-energy measurements, the ratio of the effective linear attenuation coefficients for the low-energy spectrum μ_{Low} and for the high-energy spectrum μ_{High} can be obtained from the following modified formula

$$F(Z) = \frac{\mu_{Low}(Z)}{\mu_{High}(Z)} = \left(\frac{\log\left(\int_{E_1=0}^{E_{max}} W(E_1)\, e^{-\mu(E_1,Z)\cdot t}\, dE_1 \right)}{\log\left(\int_{E_2=0}^{E_{max}} W(E_2)\, e^{-\mu(E_2,Z)\cdot t}\, dE_2 \right)} \right) \quad \ldots\ldots\ldots\ldots\ldots\ldots\ldots\ldots\ldots\ldots (7)$$

The above method is explicitly dependent on the thickness (t) of the object being inspected. As can be seen in figure 4, evaluating this formula leads to a strong dependence of the dual-energy function on the thickness, rather than the atomic number.

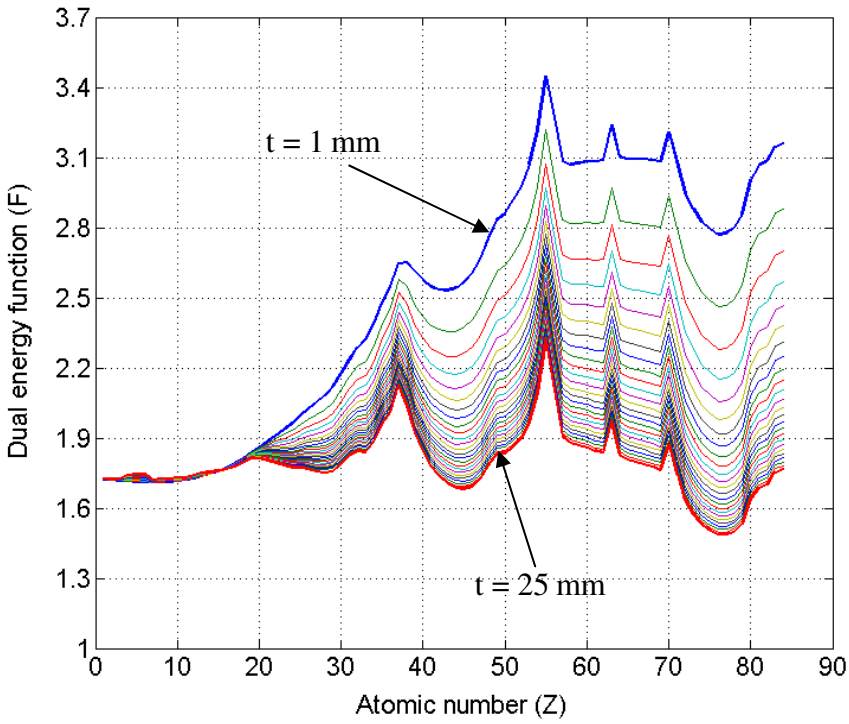

Figure 4. Variation of dual-energy function F(Z, t) with material atomic number (Z) and thickness (t).

3. Experimental Setup

In order to validate the simulation results described in section 2, we performed dual-energy measurements at the high-energy X-ray laboratory at BAM. The experimental setup used for the dual-energy measurements is shown in figure 5. A pulsed betatron with 0.6 mm thick tantalum target was used to generate high-energy X-rays with a maximum energy of 7.5 MeV at a pulse repetition frequency of 200 Hz [16]. In this study, the digital X-ray imaging was carried out using a high-resolution digital detector array (Model: Perkin Elmer XRD 1622).

The detection area of the matrix detector is 40.96 cm×40.96 cm and it consists of 2048×2048 pixels with a pixel size of 200 µm. Here, the scintillating material is gadolinium oxysulfide (Gd_2O_2S), which converts the ionizing or penetrating radiation into an electronic signal. The developed test phantom containing different low-Z (PMMA, Mg, Al) and high-Z (Fe, Cu, Sn) material step wedges is shown in figure 6. Additionally, we placed a 6 mm thick steel plate between the test phantom and the matrix detector, for the setup to more closely resemble the general cargo container inspection.

4. Results and Discussion

Figure 7 shows the comparison of an experimental dual-energy image of a test phantom with simulated results. Here, the dual-energy image is obtained after processing the low- and high-energy X-ray images. In addition, we carried out the Monte Carlo simulations of dual high-energy X-ray imaging using the aRTist simulation program. The resulting simulated dual-energy image is shown in fig. 7. A very good agreement between simulation and experiments is obtained.

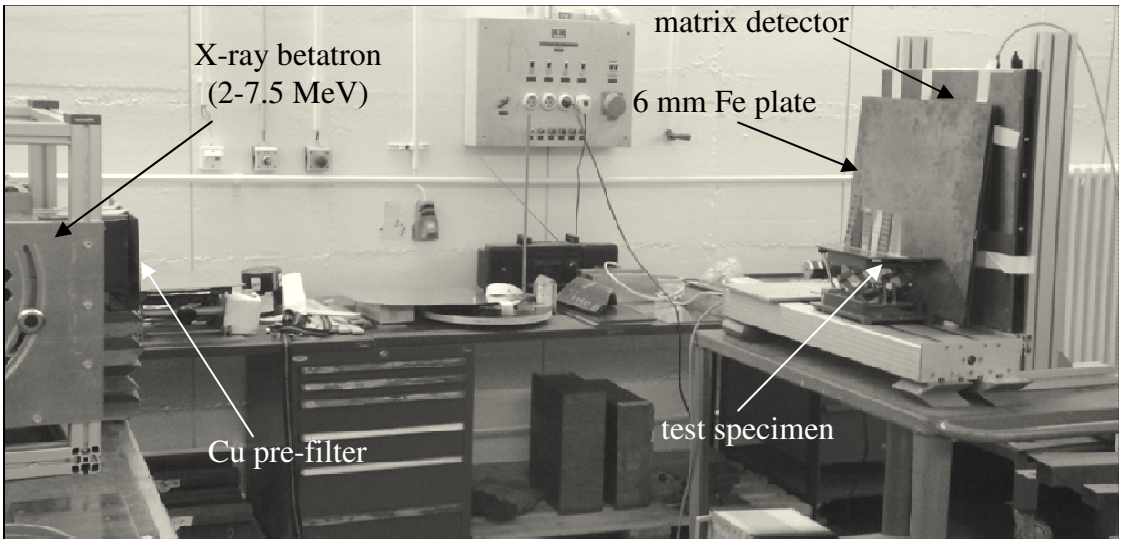

Figure 5. Experimental setup used for dual high-energy X-ray measurements.

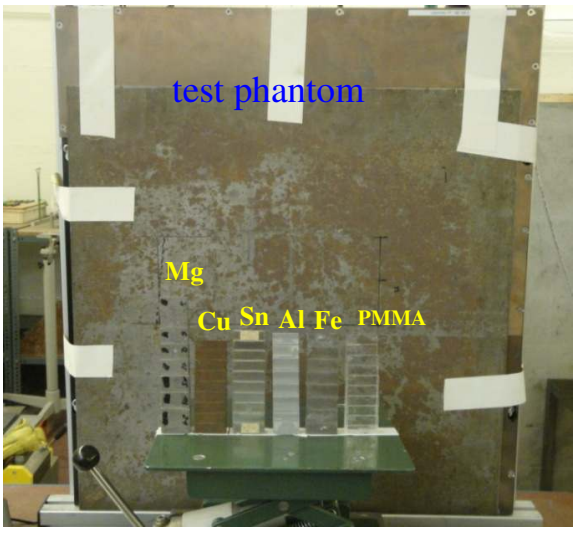

Figure 6. Test phantom showing different low- and high-Z material step wedges.

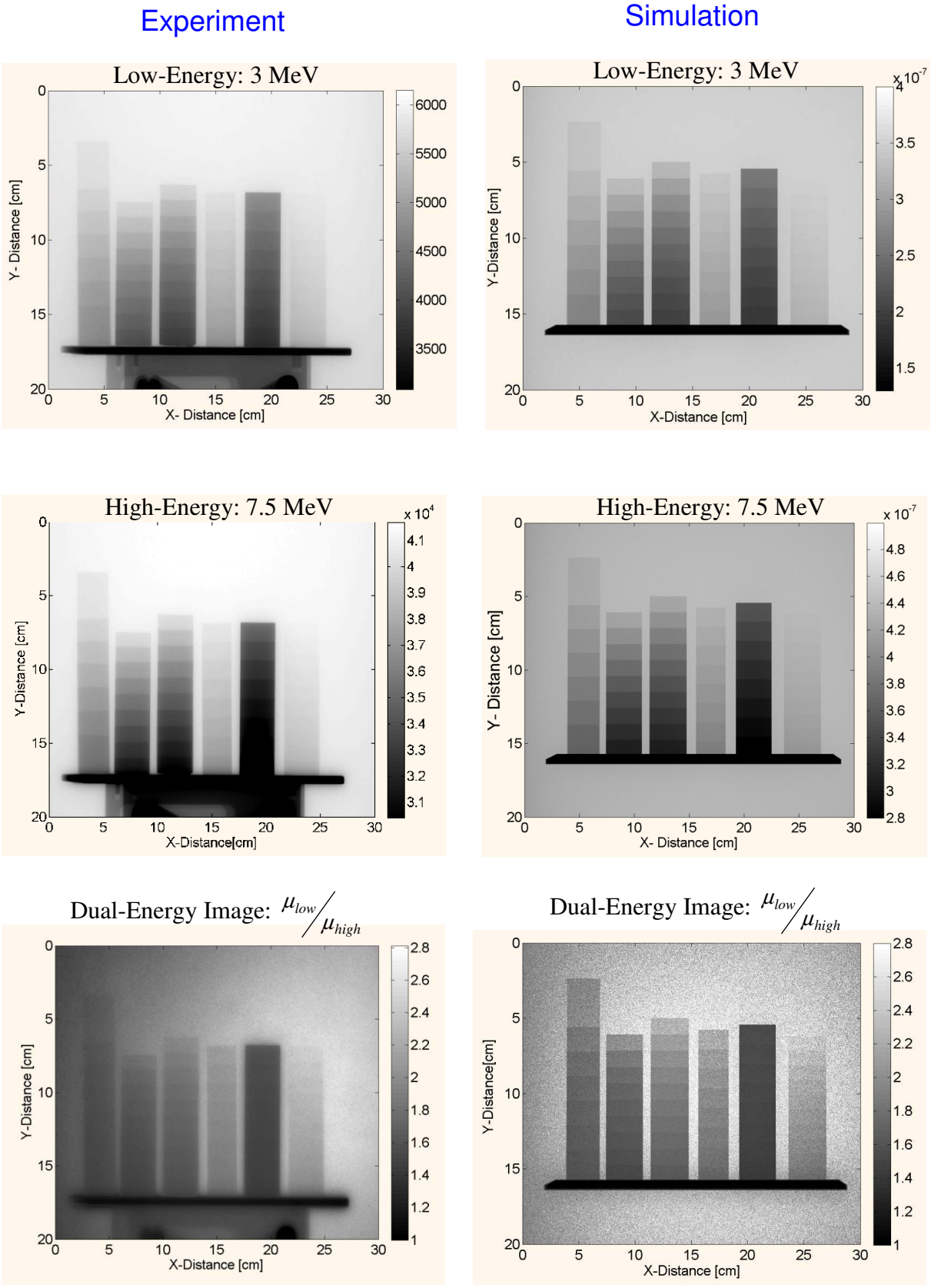

Figure 7. Comparison of experimental and simulated single-energy and dual-energy X-ray images of a test phantom containing different step wedges. The selected pre-filter material is copper with a thickness of 4 mm for the low-energy case and 10 mm for the high-energy case.

It can be seen in figure 7 that the attenuation of X-rays is strongest for the iron (Fe) step wedge compared to other materials. The quality of the dual-energy image was significantly improved by selecting optimum pre-filter thicknesses, which reduces the low-energy part of the bremsstrahlung spectrum. For the high-energy method examined here, the probability of discriminating materials diminishes with increasing material thickness. The other important factor that influences the material discrimination capability is the scattered radiation. The comparison between simulated and experimental color-coded dual-energy images is shown in figure 8. A good quantitative agreement is achieved between simulated and experimental effective attenuation coefficients for Al, Fe and PMMA. We observe minor discrepancies in case of Mg, Cu and Sn.

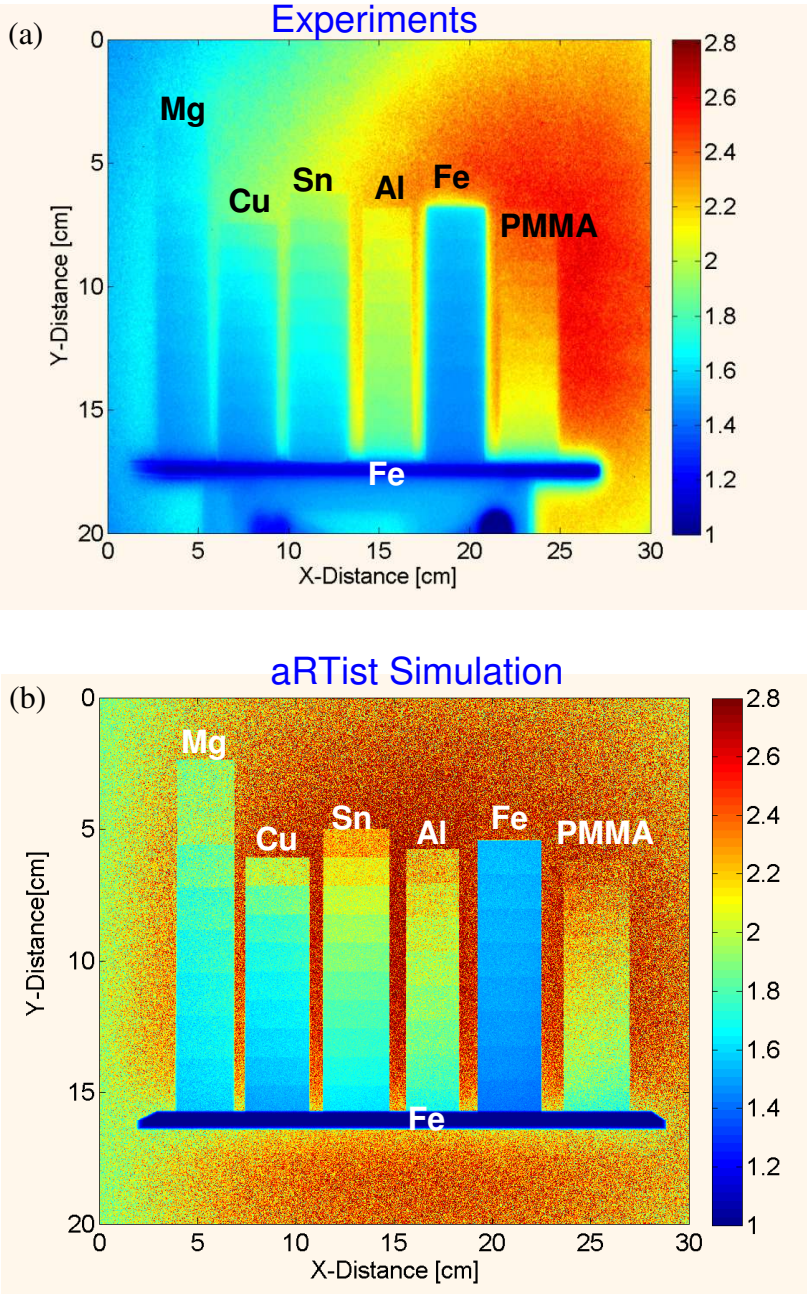

Figure 8. Color-coded dual-energy X-ray images of the test phantom, generated by applying the 'Jet' color scale.

The main reason for these minor discrepancies is a shift of the beam intensity maximum with acceleration potential of the betatron. It can be seen in fig. 8 that the beam maximum is shifted from the center in the experimental result (see large red background region in fig. 8(a)). Whereas in the simulated result, as expected, the beam maximum is concentrated well at the center (see fig. 8(b)). While a high-resolution digital detector array was used in the present dual-energy experiments, scattered radiation can be further minimized by employing line detectors, which detect only a finely collimated X-ray beam.

4. Conclusions

In conclusion, a dual high-energy X-ray imaging technique for material discrimination in cargo containers has been developed. Numerical results on the variation of the dual-energy function with atomic number at higher X-ray energies showed that the material discrimination capability is reduced for atomic numbers Z<=10 and Z>=46. We also observed that the accuracy of material discrimination in cargo containers could be improved by considering the effect of material thickness on effective attenuation coefficients. Dual-energy measurements were carried out using a portable high-energy (2-7.5 MeV) X-ray betatron and a digital detector array with high spatial resolution (400 µm). The measured dual-energy X-ray images of a test phantom containing low- and high-Z material step wedges were compared with the simulation results obtained using aRTist. A very good quantitative agreement between simulation and experiments was achieved. A thorough quantitative analysis of material discrimination in cargo containers with complex packing using dual high-energy X-ray computed tomography (CT) is under progress and will be presented in the future.

Acknowledgements

This research was financially supported by the German Federal Ministry of Education and Research (BMBF) under its research program for aviation security (Project: SiLuFra (secure air-freight transport chain) under grant number 13N12729). The authors also thank Dr. C. Bellon, Dr. G.-R. Jaenisch, and Dr. U. Zscherpel for helpful discussions.

References

1. R E Alvarez, A Macovski, ‘Energy-selective reconstructions in X-ray computerized tomography’, Phys. Med. Biol., Vol 21, pp 733-744, 1976.

2. L Yu, X Liu, C H McCollough, ‘Pre-reconstruction three-material decomposition in dual-energy CT’, Proceedings of SPIE, Medical Imaging, Vol 7258, 72583V, 2009.

2. M Bastan, M R Yousefi, T M Breuel, ‘Visual words on baggage X-ray images’, Computer Analysis of Images and Patterns, Lecture Notes in Computer Science, Vol 6854, pp 360-368, 2011.

4. R Pincu, O Kleinberger-Riedrich, ‘A review Digital Radiography in the service of security’, Proceedings of 18th World Conference of Nondestructive Testing, Durban, South Africa, April, 2012.

5. C Tang, H B Chen and Y H Liu, ‘Electron Linacs for Cargo Inspection and Other Industrial Applications’, IAEA Proceedings of International Topical Meeting on

Nuclear Research Applications and Utilization of Accelerators, Vienna, SM/EB-28, 4-8 May 2009.

6. S Orogodnikov, V Petrunin, 'Processing of interlaced images in 4-10 MeV dual energy customs system for material recognition', Physical Review Special Topics-Accelerators and Beams, Vol 5, pp 104701-11, 2002.

7. M Stein, V A Kasyanov, V A Chaklov, J Macleod, P Marjoribanks, S Hubbard, 'Small size betatrons for radiographic inspection, Proceedings of 16th World Conference on Non-Destructive Testing (WCNDT), Radiography, Montreal, Canada, 2004.

8. S Kolkoori, N Wrobel, K Osterloh, B Redmer, A Deresch and U Ewert, 'High-Energy Radiography for Detecting Details in Highly Complex Packings', Materials Testing, Vol 55, No.9, pp 683-688, 2013 (in German).

9. U Ewert., U Zscherpel, K Heyne, M Jechow, K Bavendiek, 'Image quality in digital industrial radiology', Materials Evaluation, Vol 70, No. 8, pp 955-964, 2012.

10. U Ewert, U Zscherpel, M Jechow, 'Essential parameters and conditions for optimum image quality in digital radiology', Proceedings of 18th World Conference on Nondestructive Testing (WCNDT), Durban, South Africa, 16-20 April, 2012.

11. B J Heisemann , J Lippert, K Stierstorfer, 'Density and atomic number measurements with spectral X-ray attenuation method', Journal of Applied Physics, Vol 94, No. 3, PP 2073-79, 2003.

12. X Liu, L Yu, A Primak, C. McCollough, 'Quantitaive imaging of element composition and mass fraction using dual-energy CT: Three-material decomposition', Medical Physics, Vol 36, pp 1602-9, 2009.

13. G R Tillack, C Nockemann, C Bellon, 'X-ray modelling for industrial applications', NDT & E International, Vol 33, pp 481–488, 2000.

14. C Bellon, G R Jaenisch, 'aRTist –analytical RT inspection simulation tool', Proceedings of International Symposium on Digital Industrial Radiology and Computed Tomography, Lyon, France; June 25-27, 2007.

15. A Deresch, G R Jaenisch, C Bellon, A Warrikhoff, 'Simulating X-ray Spectra: From Tube Parameters to Detector Output', Proceedings of 18th World Conference on Nondestructive Testing (WCNDT), Durban, South Africa, 16-20 April, 2012.

16. JME Portable 7.5 MeV X-ray Betatron for Radiographic Non-Destructive Testing, User Manual, Issue **1**, 2006.

17. XRD 1622 Detector Series, Basic Specifications and Potential Applications of Digital Flat Panel Detectors, http://www.perkinelmer.com